HP–ADAPTIVE COMPOSITE DISCONTINUOUS GALERKIN METHODS FOR ELLIPTIC PROBLEMS ON COMPLICATED DOMAINS

STEFANO GIANI * AND PAUL HOUSTON †

Abstract. In this paper we develop the *a posteriori* error estimation of *hp*–version discontinuous Galerkin composite finite element methods for the discretization of second–order elliptic partial differential equations. This class of methods allows for the approximation of problems posed on computational domains which may contain a huge number of local geometrical features, or micro-structures. While standard numerical methods can be devised for such problems, the computational effort may be extremely high, as the minimal number of elements needed to represent the underlying domain can be very large. In contrast, the minimal dimension of the underlying composite finite element space is *independent* of the number of geometric features. Computable bounds on the error measured in terms of a natural (mesh-dependent) energy norm are derived. Numerical experiments highlighting the practical application of the proposed estimators within an automatic *hp*–adaptive refinement procedure will be presented.

Key words. Composite finite element methods, discontinuous Galerkin methods, *a posteriori* error estimation, *hp*–adaptivity

1. Introduction. In recent years, a new class of finite elements, referred to as Composite Finite Elements (CFEs), have been developed for the numerical solution of partial differential equations, which are particularly suited to problems characterized by small details in the computational domain or micro-structures; see, for example, [10, 9], for details. The key idea of CFEs is to exploit general shaped element domains upon which elemental basis functions may only be locally piecewise smooth. In particular, an element domain within a CFE may consist of a collection of neighbouring elements present within a standard finite element method, with the basis function of the CFE being constructed as a linear combination of those defined on the standard finite element subdomains. In this way, CFEs offer an ideal mathematical and practical framework within which finite element solutions on (coarse) aggregated meshes may be defined. CFEs have been developed in the context of *h*–version conforming finite element methods by Sauter and co-workers in the series of articles [10, 9, 23]; the generalization to *hp*–version discontinuous Galerkin composite finite element methods (DGCFEMs) has been considered in our recent article [4]. We point out that the general philosophy of CFE methods is to construct the underlying finite element spaces based on first generating a hierarchy of meshes, such that the finest mesh does indeed provide an accurate representation of the underlying computational domain, followed by the introduction of appropriate prolongation operators which determine how the finite element basis functions on the coarse mesh are defined in terms of those on the fine grid.

In this article, we extend the work presented in [4] to consider the *a posteriori* error analysis of the *hp*–version DGCFEM. In particular, we shall derive a computable upper bound on the error, measured in terms of the underlying DG-energy norm, which is explicit in terms of the dependence on h and p. This upper bound is based on the general techniques developed in the articles [13, 14, 15, 17]. Indeed, here the proof crucially relies on the approximation of discontinuous finite element functions by

* School of Engineering and Computing Sciences, Durham University, South Road, Durham, DH1 3LE, UK, email: stefano.giani@durham.ac.uk.

† School of Mathematical Sciences, University of Nottingham, University Park, Nottingham NG7 2RD, UK, email: Paul.Houston@nottingham.ac.uk.

conforming ones. Results of this type have been developed independently by a number of authors in the context of the h-version of the DGFEM; see, for example, [12, 18]. Numerical experiments highlighting the performance of the proposed estimator within an hp-adaptive mesh refinement algorithm will also be presented.

The structure of this article is as follows. In Section 2, we introduce the model problem and state the necessary assumptions on the computational domain Ω. Section 3 introduces the composite finite element spaces considered in this article, based on exploiting the ideas developed in the series of articles [4, 10, 9, 23]. In Section 4 we formulate the hp–DGCFEM; the *a posteriori* analysis of the proposed method is then undertaken in Section 5. The practical performance of the proposed hp–error indicators within an automatic hp–refinement algorithm for a range of two–dimensional problems is studied in Section 6. Finally, in Section 7 we summarize the work presented in this article and draw some conclusions.

2. Model problem. In this article we consider the following model problem: given $f \in L_2(\Omega)$, find u such that

$$-\Delta u = f \quad \text{in } \Omega, \tag{2.1}$$

$$u = 0 \quad \text{on } \partial\Omega. \tag{2.2}$$

Here, Ω is a bounded, connected polyhedral domain in $\mathbb{R}^d$, $d > 1$, with boundary $\partial\Omega$; in particular, it is assumed that Ω is a 'complicated' domain, in the sense that it contains small details or micro-structures. With this in mind, throughout this article, we assume that Ω is such that the following extension result holds.

THEOREM 2.1. *Let Ω be a domain with a Lipschitz boundary. Then there exists a linear extension operator $\mathfrak{E} : H^s(\Omega) \to H^s(\mathbb{R}^d)$, $s \in \mathbb{N}_0$, such that $\mathfrak{E}v|_\Omega = v$ and*

$$\|\mathfrak{E}v\|_{H^s(\mathbb{R}^d)} \leq C\|v\|_{H^s(\Omega)},$$

where C is a positive constant depending only on s and Ω.

Proof. See Stein [25, Theorem 5, p. 181]; the extension of this result to domains which are simply connected, but may contain micro-scales, is considered in [24]. □

3. Construction of the composite finite element spaces. In this section, we outline the construction of the underlying CFE space. In particular, we construct a hierarchy of so-called reference and physical meshes. For simplicity, here we consider a simplification of the algorithm presented in [4]; indeed, [4] introduced an additional hierarchy of meshes, referred to as logical meshes. In that setting, nodes were also moved as part of the construction of the mesh hierarchy; in the current article, the physical and logical meshes coincide. We point out that, with a judicious choice of the initial background mesh, and (potentially) nonstandard element refinement, a wide range of complicated domains may be studied by simply exploiting the proposed two-mesh hierarchy. For related work, we refer to the articles [10, 9, 23].

3.1. Finite element meshes. In this section we briefly outline a general strategy to generate a hierarchy of reference and physical finite element meshes, cf. [4]. We point out that any such hierarchy of meshes may be employed within this framework to describe a complicated domain $\Omega \subset \mathbb{R}^d$; for simplicity of presentation, we assume that $d = 2$, though the general approach naturally generalizes to higher–dimensional domains.

To begin, we first need to construct a sequence of *reference* meshes, which we shall denote by $\hat{\mathcal{T}}_{h_i}$, $i = 1, \ldots, \ell$. We assume that the reference meshes are nested,

Algorithm 3.1 Refine Mesh

Set $\hat{\mathcal{T}}_{h_1} = \hat{\mathcal{T}}_H$, and the mesh counter $\ell = 1$.
Set $\hat{\mathcal{T}}_{h_{\ell+1}} = \emptyset$.
for all $\hat{\kappa} \in \hat{\mathcal{T}}_{h_\ell}$ **do**
  if $\hat{\kappa} \subset \Omega$ **then**
    $\hat{\mathcal{T}}_{h_{\ell+1}} = \hat{\mathcal{T}}_{h_{\ell+1}} \bigcup \{\hat{\kappa}\}$;
  else
    Refine $\hat{\kappa} = \bigcup_{i=1}^{n_{\hat{\kappa}}} \hat{\kappa}_i$, $n_{\hat{\kappa}} \geq 1$.
    for $i = 1, \ldots, n_{\hat{\kappa}}$ **do**
      if $\hat{\kappa}_i \cap \Omega \neq \emptyset$ **then**
        Set $\hat{\mathcal{T}}_{h_{\ell+1}} = \hat{\mathcal{T}}_{h_{\ell+1}} \bigcup \{\hat{\kappa}_i\}$.
      end if
    end for
  end if
end for
Perform additional refinement of elements in $\hat{\mathcal{T}}_{h_{\ell+1}}$ to undertake appropriate mesh smoothing, e.g., to ensure that the resulting mesh is 1–irregular, etc. For further details on this issue, we refer to [4].
if Reference mesh $\hat{\mathcal{T}}_{h_\ell}$ is *sufficiently* fine, in the sense that it provides an accurate representation of the boundary of Ω **then**
  `STOP`.
else
  Set $\ell = \ell + 1$, and `GOTO` 2.
end if

in the sense that every element $\hat{\kappa}_i \in \hat{\mathcal{T}}_{h_i}$, $i = 1, \ldots, \ell - 1$, is a parent of a subset of elements which belong to the finer mesh $\hat{\mathcal{T}}_{h_j}$, where $j = i + 1, \ldots, \ell$, respectively. To this end, we proceed as follows: we define a coarse conforming shape–regular mesh $\hat{\mathcal{T}}_H = \{\hat{\kappa}\}$, consisting of (standard) closed elements $\hat{\kappa}$, whose open intersection is empty. By *standard* element domains, we mean quadrilaterals/triangles in two dimensions ($d = 2$), and tetrahedra/hexahedra when $d = 3$. Here, we assume that $\hat{\mathcal{T}}_H$ is a non-boundary fitting mesh is the sense that it does *not* resolve the boundary of the computational domain Ω. More precisely, we assume that $\hat{\mathcal{T}}_H$ satisfies the following condition:

$$\Omega \subset \Omega_H = \left(\bigcup_{\hat{\kappa} \in \hat{\mathcal{T}}_H} \hat{\kappa} \right)^\circ \qquad \text{and} \qquad \hat{\kappa}^\circ \cap \Omega \neq \emptyset \ \forall \hat{\kappa} \in \hat{\mathcal{T}}_H,$$

where, for a closed set $D \subset \mathbb{R}^d$, D° denotes the interior of D, cf. [23], for example. The finite element mesh $\hat{\mathcal{T}}_H$ should be viewed as having a granularity that is affordable for which to solve our underlying problem, though is far too coarse to actually represent the underlying geometry Ω.

Given $\hat{\mathcal{T}}_H$, we now construct a sequence of successively refined (nested) computational meshes using Algorithm 3.1. We stress that Algorithm 3.1 simply provides a prototype of a typical refinement algorithm that could be employed to generate the sequence of nested reference meshes $\{\hat{\mathcal{T}}_{h_i}\}_{i=1}^{\ell}$; alternative sequences of grids may also be exploited. We implicitly assume that element refinements are undertaken in such a manner to ensure that the boundary of the computational domain is precisely

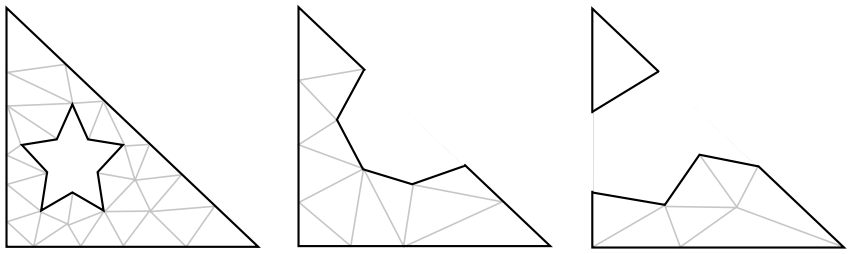

FIG. 3.1. *Composite finite element domains (black lines), together with the underlying reference fine mesh (grey lines).*

described by the finest reference mesh $\hat{\mathcal{T}}_{h_\ell}$.

We recall that the reference meshes $\{\hat{\mathcal{T}}_{h_i}\}_{i=1}^{\ell}$ are nested, cf. above. Formally, we write this as follows: given $\hat{\kappa}_i \in \hat{\mathcal{T}}_{h_i}$, for some i, where $2 \leq i \leq \ell$, the parent element $\hat{\kappa}_{i-1} \in \hat{\mathcal{T}}_{h_{i-1}}$ such that $\hat{\kappa}_i \subset \hat{\kappa}_{i-1}$ is given by the mapping

$$\mathfrak{F}_{i-1}^{i}(\hat{\kappa}_i) = \hat{\kappa}_{i-1}.$$

Thereby, the mapping $\mathfrak{F}_i^\ell = \mathfrak{F}_i^{i+1} \circ \mathfrak{F}_{i+1}^{i+2} \circ \ldots \circ \mathfrak{F}_{\ell-1}^{\ell}$, provides the link between the parent elements on the reference mesh $\hat{\mathcal{T}}_{h_i}$, $i = 1, \ldots, \ell-1$, with its children on the finest reference mesh $\hat{\mathcal{T}}_{h_\ell}$. More precisely, given an element $\hat{\kappa}_\ell \in \hat{\mathcal{T}}_{h_\ell}$, the parent element $\hat{\kappa}_i \in \hat{\mathcal{T}}_{h_i}$, $i = 1, \ldots, \ell-1$, which satisfies $\hat{\kappa}_\ell \subset \hat{\kappa}_i$ is given by:

$$\mathfrak{F}_i^\ell(\hat{\kappa}_\ell) = \hat{\kappa}_i.$$

We now proceed to define the sequence of physical meshes $\mathcal{T}_{h_i}$, $i = 1, \ldots, \ell$. To this end, we define the finest physical mesh $\mathcal{T}_{h_\ell}$ to be equal to the finest reference mesh $\hat{\mathcal{T}}_{h_\ell}$, i.e., $\mathcal{T}_{h_\ell} = \hat{\mathcal{T}}_{h_\ell}$. The newly created finest physical mesh $\mathcal{T}_{h_\ell}$ is a *standard* boundary conforming mesh upon which standard finite element/finite volume methods may be applied. In the current context, we assume that the geometry is *complicated* in the sense that $\mathcal{T}_{h_\ell}$ is too fine to undertake computations. Instead, we wish to only use $\mathcal{T}_{h_\ell}$ to create a coarse composite finite element mesh $\mathcal{T}_{\mathtt{CFE}}$ upon which numerical simulations will be performed.

With this construction, we may now naturally create a hierarchy of physical meshes $\{\mathcal{T}_{h_i}\}_{i=1}^{\ell}$ by simply coarsening $\mathcal{T}_{h_\ell}$. In order to ensure that these meshes are nested, the element domains within these meshes may consist of general polygons. To this end, we write

$$\begin{aligned}\mathcal{T}_{h_i} = \{\kappa : \kappa = \cup\kappa_\ell,\ \kappa_\ell \in \mathcal{T}_{h_\ell},\ & \text{ which share a common parent from mesh level } i, \text{ i.e.,} \\ & \mathfrak{F}_i^\ell(\kappa_\ell) \text{ is identical for all members of this set}\},\end{aligned}$$

$i = 1, \ldots, \ell-1$. We refer to the coarsest level physical mesh $\mathcal{T}_{h_1}$ as the *composite finite element mesh*; in particular, we denote this by $\mathcal{T}_{\mathtt{CFE}}$, i.e., $\mathcal{T}_{\mathtt{CFE}} = \mathcal{T}_{h_1}$. We stress that the elements $\kappa \in \mathcal{T}_{\mathtt{CFE}}$ consist of general polygons; cf. Figure 3.1 for examples of potential element configurations, together with the underlying fine reference mesh $\hat{\mathcal{T}}_{h_\ell}$.

3.2. Finite element spaces. Given the meshes $\{\hat{\mathcal{T}}_{h_i}\}_{i=1}^{\ell}$ and $\{\mathcal{T}_{h_i}\}_{i=1}^{\ell}$, we define the corresponding sequences of reference and physical discontinuous Galerkin

finite element spaces $V(\hat{\mathcal{T}}_{h_i}, \hat{\boldsymbol{p}})$ and $V(\mathcal{T}_{h_i}, \boldsymbol{p})$, $i = 1, \ldots, \ell$, respectively, consisting of piecewise discontinuous polynomials. To this end, we first construct the coarsest reference space $V(\hat{\mathcal{T}}_{h_1}, \hat{\boldsymbol{p}}) \equiv V(\hat{\mathcal{T}}_H, \hat{\boldsymbol{p}})$. For each $\hat{\kappa} \in \hat{\mathcal{T}}_{h_1}$, we assign a polynomial degree $p_{\hat{\kappa}}$. Writing $\hat{\boldsymbol{p}} = \{p_{\hat{\kappa}} : \hat{\kappa} \in \hat{\mathcal{T}}_{h_1}\}$, we define

$$V(\hat{\mathcal{T}}_{h_1}, \hat{\boldsymbol{p}}) = \{u \in L_2(\Omega_H) : u|_{\hat{\kappa}} \in \mathcal{P}_{p_{\hat{\kappa}}}(\hat{\kappa}) \; \forall \hat{\kappa} \in \hat{\mathcal{T}}_{h_1}\},$$

where $\mathcal{P}_p(\hat{\kappa})$ denotes the set of polynomials of degree at most $p \geq 1$ defined over $\hat{\kappa}$. With the coarsest reference finite element space defined, the sequence of spaces $V(\hat{\mathcal{T}}_{h_i}, \hat{\boldsymbol{p}})$, $i = 2, 3, \ldots, \ell$, are constructed so that the child elements inherit the same polynomial degree assigned to their parent element. More precisely, we write

$$V(\hat{\mathcal{T}}_{h_i}, \hat{\boldsymbol{p}}) = \{u \in L_2(\Omega_{h_i}) : u|_{\hat{\kappa}} \in \mathcal{P}_{p_{\hat{\kappa}_1}}(\hat{\kappa}), \quad \text{where } \hat{\kappa}_1 = \mathfrak{F}_1^i(\hat{\kappa}) \;\; \forall \hat{\kappa} \in \hat{\mathcal{T}}_{h_i}\},$$

where $\Omega_{h_i} = \left(\bigcup_{\hat{\kappa} \in \hat{\mathcal{T}}_{h_i}} \hat{\kappa}\right)^{\circ}$, $i = 2, 3, \ldots, \ell$. Under the foregoing assumptions, we note that $\Omega_{h_\ell} \equiv \Omega$.

The composite finite element spaces are now constructed based on employing the polynomial degree vector $\boldsymbol{p} = \{p_\kappa : p_\kappa = p_{\hat{\kappa}}, \kappa \subset \hat{\kappa}, \; \hat{\kappa} \in \hat{\mathcal{T}}_{h_1}, \; \forall \kappa \in \mathcal{T}_{h_1}\}$. Thereby,

$$V(\mathcal{T}_{h_1}, \boldsymbol{p}) = \{u \in L_2(\Omega) : u|_\kappa \in \mathcal{P}_{p_\kappa}(\kappa) \; \forall \kappa \in \mathcal{T}_{h_1}\},$$

and

$$V(\mathcal{T}_{h_i}, \boldsymbol{p}) = \{u \in L_2(\Omega) : u|_\kappa \in \mathcal{P}_{p_{\kappa_1}}(\kappa), \quad \text{where } \kappa \subset \kappa_1, \; \kappa_1 \in \mathcal{T}_{h_1}, \quad \forall \kappa \in \mathcal{T}_{h_i}\},$$

$i = 2, 3, \ldots, \ell$. Thereby, noting that the meshes $\{\mathcal{T}_{h_i}\}_{i=1}^{\ell}$ are nested, we deduce that $V(\mathcal{T}_{h_1}, \boldsymbol{p}) \subseteq V(\mathcal{T}_{h_2}, \boldsymbol{p}) \subseteq \ldots \subseteq V(\mathcal{T}_{h_\ell}, \boldsymbol{p})$.

We now refer to $V(\mathcal{T}_{h_1}, \boldsymbol{p})$ as the composite finite element space $V(\mathcal{T}_{\mathtt{CFE}}, \boldsymbol{p})$, i.e., $V(\mathcal{T}_{\mathtt{CFE}}, \boldsymbol{p}) = V(\mathcal{T}_{h_1}, \boldsymbol{p})$.

4. Composite discontinuous Galerkin finite element method. In this section, we introduce the *hp*-version of the (symmetric) interior penalty DGCFEM for the numerical approximation of (2.1)–(2.2). To this end, we first introduce the following notation.

We denote by $\mathcal{F}^{\mathcal{I}}(\mathcal{T}_{\mathtt{CFE}})$ the set of all interior faces of the partition $\mathcal{T}_{\mathtt{CFE}}$ of Ω, and by $\mathcal{F}^{\mathcal{B}}(\mathcal{T}_{\mathtt{CFE}})$ the set of all boundary faces of $\mathcal{T}_{\mathtt{CFE}}$. Furthermore, we define $\mathcal{F}(\mathcal{T}_{\mathtt{CFE}}) = \mathcal{F}^{\mathcal{I}}(\mathcal{T}_{\mathtt{CFE}}) \cup \mathcal{F}^{\mathcal{B}}(\mathcal{T}_{\mathtt{CFE}})$. We emphasize that the term 'faces', of a given composite element $\kappa \in \mathcal{T}_{\mathtt{CFE}}$, consists of straight/coplanar $(d-1)$–dimensional segments of the polygonal/polyhedral domain κ. The boundary $\partial\kappa$ of an element κ and the sets $\partial\kappa \setminus \partial\Omega$ and $\partial\kappa \cap \partial\Omega$ will be identified in a natural way with the corresponding subsets of $\mathcal{F}(\mathcal{T}_{\mathtt{CFE}})$. Let κ^+ and κ^- be two adjacent elements of $\mathcal{T}_{\mathtt{CFE}}$, and $\mathbf{x}$ an arbitrary point on the interior face $F \in \mathcal{F}^{\mathcal{I}}(\mathcal{T}_{\mathtt{CFE}})$ given by $F = \partial\kappa^+ \cap \partial\kappa^-$. Furthermore, let v and $\mathbf{q}$ be scalar- and vector-valued functions, respectively, that are smooth inside each element $\kappa^\pm$. By $(v^\pm, \mathbf{q}^\pm)$, we denote the traces of $(v, \mathbf{q})$ on F taken from within the interior of $\kappa^\pm$, respectively. Then, the averages of v and $\mathbf{q}$ at $\mathbf{x} \in F$ are given by

$$\{\!\{v\}\!\} = \frac{1}{2}(v^+ + v^-), \qquad \{\!\{\mathbf{q}\}\!\} = \frac{1}{2}(\mathbf{q}^+ + \mathbf{q}^-),$$

respectively. Similarly, the jumps of v and $\mathbf{q}$ at $\mathbf{x} \in F$ are given by

$$[\![v]\!] = v^+ \, \mathbf{n}_{\kappa^+} + v^- \, \mathbf{n}_{\kappa^-}, \qquad [\![\mathbf{q}]\!] = \mathbf{q}^+ \cdot \mathbf{n}_{\kappa^+} + \mathbf{q}^- \cdot \mathbf{n}_{\kappa^-},$$

respectively, where we denote by $\mathbf{n}_{\kappa^\pm}$ the unit outward normal vector of $\partial\kappa^\pm$, respectively. On a boundary face $F \in \mathcal{F}^{\mathcal{B}}(\mathcal{T}_{\mathtt{CFE}})$, we set $\{\!\{v\}\!\} = v$, $\{\!\{\mathbf{q}\}\!\} = \mathbf{q}$, and $[\![v]\!] = v\mathbf{n}$, with $\mathbf{n}$ denoting the unit outward normal vector on the boundary $\partial\Omega$.

With this notation, we make the following key assumptions:

(A1) For all elements $\kappa \in \mathcal{T}_{\mathtt{CFE}}$, we define

$$C_\kappa = \mathrm{card}\left\{F \in \mathcal{F}(\mathcal{T}_{\mathtt{CFE}}) : F \subset \partial\kappa\right\}.$$

In the following we assume that there exists a positive constant C_F such that

$$\max_{\kappa\in\mathcal{T}_{\mathtt{CFE}}} C_\kappa \leq C_F,$$

uniformly with respect to the mesh size.

(A2) Given the construction of the reference meshes $\hat{\mathcal{T}}_{h_i}$, $i = 1, 2, \ldots, \ell$, we assume that the finest mesh $\hat{\mathcal{T}}_{h_\ell}$ is the *minimal mesh representation* of the domain Ω in the following sense. Given a face $F \in \mathcal{F}(\mathcal{T}_{\mathtt{CFE}})$ of an element $\kappa \in \mathcal{T}_{\mathtt{CFE}}$, i.e., $F \subset \partial\kappa$, we assume there is a constant $\rho_1 \geq 1$ such that

$$\rho_1^{-1} \leq h_F/h_{\hat{\kappa}} \leq \rho_1 \quad \forall \hat{\kappa} \in \mathcal{S}_\kappa = \{\hat{\kappa} \in \hat{\mathcal{T}}_{h_\ell} :\ \hat{\kappa} \subset \kappa\},$$

where h_F and $h_{\hat{\kappa}}$ denote the diameter of F and $\hat{\kappa}$, respectively.

(A3) We assume that the polynomial degree vector $\boldsymbol{p}$ is of bounded local variation, that is, there is a constant $\rho_2 \geq 1$ such that

$$\rho_2^{-1} \leq p_\kappa/p_{\kappa'} \leq \rho_2,$$

whenever κ and κ' share a common face ($(d-1)$–dimensional facet).

We remark that, as an immediate consequence of Assumption (A2), the following inverse inequality holds: given a face $F \in \mathcal{F}(\mathcal{T}_{\mathtt{CFE}})$ of an element $\kappa \in \mathcal{T}_{\mathtt{CFE}}$, there exists a positive constant C_{inv}, independent of the local mesh size and local polynomial order, such that

$$\|\nabla v\|^2_{L_2(F)} \leq C_{\mathrm{inv}} \frac{p_\kappa^2}{h_F} \|\nabla v\|^2_{L_2(\kappa)} \tag{4.1}$$

for all $v \in V(\mathcal{T}_{\mathtt{CFE}}, \boldsymbol{p})$, cf. [4].

With this notation, we consider the (symmetric) interior penalty hp–DGCFEM for the numerical approximation of (2.1)–(2.2): find $u_h \in V(\mathcal{T}_{\mathtt{CFE}}, \boldsymbol{p})$ such that

$$B_{\mathtt{DG}}(u_h, v) = F_h(v) \tag{4.2}$$

for all $v \in V(\mathcal{T}_{\mathtt{CFE}}, \boldsymbol{p})$, where

$$\begin{aligned} B_{\mathtt{DG}}(u, v) = &\sum_{\kappa\in\mathcal{T}_{\mathtt{CFE}}} \int_\kappa \nabla u \cdot \nabla v \, d\mathbf{x} - \sum_{F\in\mathcal{F}(\mathcal{T}_{\mathtt{CFE}})} \int_F \left(\{\!\{\nabla_h v\}\!\} \cdot [\![u]\!] + \{\!\{\nabla_h u\}\!\} \cdot [\![v]\!]\right) ds \\ &+ \sum_{F\in\mathcal{F}(\mathcal{T}_{\mathtt{CFE}})} \int_F \sigma \, [\![u]\!] \cdot [\![v]\!] \, ds, \\ F_h(v) = &\int_\Omega f v \, d\mathbf{x}. \end{aligned}$$

Here, ∇_h denotes the elementwise gradient operator. Furthermore, the function $\sigma \in L_\infty(\mathcal{F}(\mathcal{T}_{\mathtt{CFE}}))$ is the discontinuity stabilization function that is chosen as follows: we define the function $\mathtt{p} \in L_\infty(\mathcal{F}(\mathcal{T}_{\mathtt{CFE}}))$ by

$$\mathtt{p}(\mathbf{x}) := \begin{cases} \max(p_\kappa, p_{\kappa'}), & \mathbf{x} \in F \in \mathcal{F}^{\mathcal{I}}(\mathcal{T}_{\mathtt{CFE}}),\ F = \partial\kappa \cap \partial\kappa', \\ p_\kappa, & \mathbf{x} \in F \in \mathcal{F}^{\mathcal{B}}(\mathcal{T}_{\mathtt{CFE}}),\ F \subset \partial\kappa \cap \partial\Omega, \end{cases}$$

and set

$$\sigma|_F = \gamma \mathtt{p}^2 h_F^{-1}, \tag{4.3}$$

with a parameter $\gamma > 0$ that is independent of h_F and $\mathbf{p}$.

We conclude this section by equipping the composite finite element space $V(\mathcal{T}_{\mathtt{CFE}}, \boldsymbol{p})$ with the DG energy norm $|||\cdot|||_{\mathtt{DG}}$ defined by

$$|||\, v \,|||_{\mathtt{DG}}^2 = \sum_{\kappa \in \mathcal{T}_{\mathtt{CFE}}} \|\nabla v\|_{L_2(\kappa)}^2 + \sum_{F \in \mathcal{F}(\mathcal{T}_{\mathtt{CFE}})} \|\sigma^{1/2} [\![v]\!]\|_{L_2(F)}^2.$$

The stability and *a priori* error analysis of the *hp*–DGCFEM defined by (4.2) has been undertaken in our recent article [4]; in particular, we note that the discrete problem is well–posed only if γ is chosen to be sufficiently large.

5. *A posteriori* error analysis. In this section, we develop the *a posteriori* error analysis of the *hp*–DGCFEM defined by (4.2). To this end, we denote by Π the L_2–projection operator onto $V(\mathcal{T}_{\mathtt{CFE}}, \boldsymbol{p})$; with this notation, we state the following upper bound.

THEOREM 5.1. *Let the analytical solution u of* (2.1)–(2.2) *belong to $H_0^1(\Omega)$. Furthermore, let $u_h \in V(\mathcal{T}_{\mathtt{CFE}}, \boldsymbol{p})$ be its composite discontinuous Galerkin approximation defined by* (4.2). *Then, the following hp–version* a posteriori *error bound holds:*

$$|||\, u - u_h \,|||_{\mathtt{DG}} \leq C \left(\sum_{\kappa \in \mathcal{T}_{\mathtt{CFE}}} (\eta_\kappa^2 + \mathcal{O}_\kappa^2) \right)^{\frac{1}{2}}, \tag{5.1}$$

where the local error indicators η_κ, $\kappa \in \mathcal{T}_{\mathtt{CFE}}$, are defined by

$$\begin{aligned} \eta_\kappa^2 = {} & h_\kappa^2 p_\kappa^{-2} \|\Pi f + \Delta u_h\|_{L_2(\kappa)}^2 \\ & + \sum_{F \subset \partial\kappa \setminus \partial\Omega} h_\kappa^2 h_F^{-1} p_\kappa^{-1} \|[\![\nabla u_h]\!]\|_{L_2(F)}^2 + \sigma h_\kappa^2 h_F^{-2} p_\kappa \|[\![u_h]\!]\|_{L_2(\partial\kappa)}^2, \end{aligned} \tag{5.2}$$

and the data oscillation term $\mathcal{O}_\kappa$ is given by

$$\mathcal{O}_\kappa = h_\kappa^2 p_\kappa^{-2} \|f - \Pi f\|_{L_2(\kappa)}^2.$$

Here, $C > 0$ is a constant that is independent of discretization parameters, and only depends on the shape-regularity of the mesh and the constants C_F, ρ_1, and ρ_2 from Assumptions (A1), (A2), and (A3), respectively.

REMARK 5.2. *Theorem 5.1 represents the generalization of the analogous* a posteriori *error bound derived in [15] for the standard discontinuous Galerkin finite element approximation of* (2.1)–(2.2), *to the composite setting. In particular, we note that the flux jump and penalty terms arising in the definition of the error indicator* (5.2) *are suitably modified to take into account the face dimension h_F; for standard element*

domains, $h_F \approx h_\kappa$, in which case the flux and penalty terms contain the usual scaling of h_κ and h_κ^{-1}, respectively.

REMARK 5.3. *In order to incorporate the inhomogeneous boundary condition $u = g$ on $\partial\Omega$, the error indicators η_κ are simply adjusted by modifying the jump indicators on $\partial\kappa \cap \partial\Omega$, with the inclusion of an additional data-oscillation term; for details, see [15].*

REMARK 5.4. *The derivation of (local) lower bounds crucially depends on exploiting suitable (weighted) inverse inequalities on general polygonal/polyhedral (possibly disconnected) element domains, cf. [19, 15] for the case when standard element shapes are employed. Initial work in this direction has been pursued in the recent article [6].*

5.1. Proof of Theorem 5.1. In this section we present the proof of the upper bound stated in Theorem 5.1.

5.1.1. DG decompositions. The proceeding proof is based on employing an *hp*–version decomposition result for the finest (reference) finite element space $V(\hat{\mathcal{T}}_{h_\ell}, \hat{\boldsymbol{p}})$. To this end, for simplicity, we assume that the finest reference mesh $\hat{\mathcal{T}}_{h_\ell}$ is conforming, i.e., it does not contain any hanging nodes; we remark that meshes containing hanging nodes can be admitted, based on exploiting the hierarchical construction studied in [17, 29, 28]. Writing $\mathcal{F}(\hat{\mathcal{T}}_{h_\ell})$ to denote the set of all faces of the partition $\hat{\mathcal{T}}_{h_\ell}$ of Ω, we define the discontinuity stabilization function $\hat{\sigma}$ on $\mathcal{F}(\hat{\mathcal{T}}_{h_\ell})$ by

$$\hat{\sigma} = \gamma\, \hat{\mathtt{p}}^2\, \hat{\mathtt{h}}^{-1}.$$

Here, $\hat{\mathtt{p}} \in L_\infty(\mathcal{F}(\hat{\mathcal{T}}_{h_\ell}))$ is defined in an analogous fashion to $\mathtt{p}$; indeed,

$$\hat{\mathtt{p}}(\mathbf{x}) := \begin{cases} \max(p_{\hat{\kappa}}, p_{\hat{\kappa}'}), & \mathbf{x} \in F = \partial\hat{\kappa} \cap \partial\hat{\kappa}', \\ p_{\hat{\kappa}}, & \mathbf{x} \in F \subset \partial\hat{\kappa} \cap \partial\Omega. \end{cases}$$

Similarly, $\hat{\mathtt{h}} \in L_\infty(\mathcal{F}(\hat{\mathcal{T}}_{h_\ell}))$ is given by

$$\hat{\mathtt{h}}(\mathbf{x}) := \begin{cases} \min(h_{\hat{\kappa}}, h_{\hat{\kappa}'}), & \mathbf{x} \in\ F = \partial\hat{\kappa} \cap \partial\hat{\kappa}', \\ h_{\hat{\kappa}}, & \mathbf{x} \in\ F \subset \partial\hat{\kappa} \cap \partial\Omega. \end{cases}$$

Furthermore, on $\hat{\mathcal{T}}_{h_\ell}$, we define the norm

$$|||\, v\, |||^2_{\widehat{\mathtt{DG}}} = \sum_{\kappa \in \hat{\mathcal{T}}_{h_\ell}} \|\nabla v\|^2_{L_2(\kappa)} + \sum_{F \in \mathcal{F}(\hat{\mathcal{T}}_{h_\ell})} \|\hat{\sigma}^{1/2} [\![v]\!]\|^2_{L_2(F)}.$$

We write $V^c(\hat{\mathcal{T}}_{h_\ell}, \hat{\boldsymbol{p}}) = V(\hat{\mathcal{T}}_{h_\ell}, \hat{\boldsymbol{p}}) \cap H^1_0(\Omega)$. The orthogonal complement of $V^c(\hat{\mathcal{T}}_{h_\ell}, \hat{\boldsymbol{p}})$ in $V(\hat{\mathcal{T}}_{h_\ell}, \hat{\boldsymbol{p}})$ with respect to the norm $|||\cdot|||_{\widehat{\mathtt{DG}}}$ is denoted by $V^\perp(\hat{\mathcal{T}}_{h_\ell}, \hat{\boldsymbol{p}})$, such that

$$V(\hat{\mathcal{T}}_{h_\ell}, \hat{\boldsymbol{p}}) = V^c(\hat{\mathcal{T}}_{h_\ell}, \hat{\boldsymbol{p}}) \oplus V^\perp(\hat{\mathcal{T}}_{h_\ell}, \hat{\boldsymbol{p}}).$$

With this notation, the following approximation result holds.

PROPOSITION 5.5. *There is an approximant $\mathcal{A} : V(\hat{\mathcal{T}}_{h_\ell}, \hat{\boldsymbol{p}}) \to V^c(\hat{\mathcal{T}}_{h_\ell}, \hat{\boldsymbol{p}})$ that satisfies*

$$\|\nabla_h (v - \mathcal{A}v)\|^2_{L_2(\Omega)} \leq C \sum_{F \in \mathcal{F}(\hat{\mathcal{T}}_{h_\ell})} \int_F \hat{\mathtt{p}}^2 \hat{\mathtt{h}}^{-1} |[\![v]\!]|^2\, ds, \qquad v \in V(\hat{\mathcal{T}}_{h_\ell}, \hat{\boldsymbol{p}}),$$

with a constant $C > 0$ that is independent of the mesh size and polynomial degrees.

Proof. For $d = 2$, we refer to [15, 17]; see also [29] for 1–irregular quadrilateral meshes. For $d = 3$, meshes consisting of 1–irregular hexahedral elements have been considered in [28]. □

Noting that $V(\mathcal{T}_{\mathtt{CFE}}, \boldsymbol{p}) \subseteq V(\hat{\mathcal{T}}_{h_\ell}, \hat{\boldsymbol{p}})$, the DG-solution $u_h \in V(\mathcal{T}_{\mathtt{CFE}}, \boldsymbol{p})$ obtained by (4.2) may be split accordingly,

$$u_h = u_h^c + u_h^\perp, \tag{5.3}$$

where $u_h^c \in V^c(\hat{\mathcal{T}}_{h_\ell}, \hat{\boldsymbol{p}})$ and $u_h^\perp \in V^\perp(\hat{\mathcal{T}}_{h_\ell}, \hat{\boldsymbol{p}})$. Furthermore, we define the error of the *hp*–DGCFEM by

$$e_h = u - u_h \equiv e_h^c - u_h^\perp, \tag{5.4}$$

where

$$e_h^c = u - u_h^c \in H_0^1(\Omega). \tag{5.5}$$

With this notation, employing Proposition 5.5, we immediately deduce the following result.

PROPOSITION 5.6. *With $u_h^\perp$ and e_h^c defined by* (5.3) *and* (5.4)*, respectively, the following bounds hold:*

$$\|\nabla_h u_h^\perp\|_{L_2(\Omega)} \leq C \left(\sum_{F \in \mathcal{F}(\mathcal{T}_{\mathtt{CFE}})} \int_F \mathtt{p}^2 h_F^{-1} |[\![v]\!]|^2 \, ds \right)^{1/2}, \qquad \|\nabla e_h^c\|_{L_2(\Omega)} \leq C |||\, e_h \,|||_{\mathtt{DG}},$$

where C is a positive constant which is independent of the discretization parameters.

Proof. Consider the proof of the first inequality: to this end, application of Proposition 5.5 gives

$$\|\nabla_h u_h^\perp\|_{L_2(\Omega)} = \|\nabla_h (u_h - u_h^c)\|_{L_2(\Omega)} \leq C \sum_{F \in \mathcal{F}(\hat{\mathcal{T}}_{h_\ell})} \int_F \hat{\mathtt{p}}^2 \hat{\mathtt{h}}^{-1} |[\![u_h]\!]|^2 \, ds.$$

Again, noting that $V(\mathcal{T}_{\mathtt{CFE}}, \boldsymbol{p}) \subseteq V(\hat{\mathcal{T}}_{h_\ell}, \hat{\boldsymbol{p}})$, we deduce that for $F \in \mathcal{F}(\hat{\mathcal{T}}_{h_\ell}) \backslash \mathcal{F}(\mathcal{T}_{\mathtt{CFE}})$, $[\![u_h]\!]|_F = \mathbf{0}$. Moreover, exploiting Assumption (A2), together with the definition of the polynomial degree vector $\boldsymbol{p}$, gives

$$\|\nabla_h u_h^\perp\|_{L_2(\Omega)} \leq C \left(\sum_{F \in \mathcal{F}(\mathcal{T}_{\mathtt{CFE}})} \int_F \mathtt{p}^2 h_F^{-1} |[\![u_h]\!]|^2 \, ds \right)^{1/2},$$

as required.

The second bound follows from the triangle inequality, the bound for $\|\nabla_h u_h^\perp\|_{L_2(\Omega)}$, together with the fact that $u \in H_0^1(\Omega)$; cf. [17], for details. □

Next, we develop the approximation results needed for the forthcoming *a posteriori* error estimation. To this end, given $\kappa \in \mathcal{T}_{\mathtt{CFE}}$, we write $\hat{\kappa} \in \hat{\mathcal{T}}_{h_1}$ to denote the element in the reference mesh $\hat{\mathcal{T}}_{h_1}$ such that $\kappa \subseteq \hat{\kappa}$. With this notation, we now recall the following approximation result.

LEMMA 5.7. *Given $v|_{\hat{\kappa}} \in H^1(\hat{\kappa})$, for $\hat{\kappa} \in \hat{\mathcal{T}}_{h_1}$, there exists $\hat{\mathcal{I}} v$ in $\mathcal{P}_{p_{\hat{\kappa}}}(\hat{\kappa})$, $p_{\hat{\kappa}} = 1, 2, \ldots,$ such that*

$$h_{\hat{\kappa}}^{-1} p_{\hat{\kappa}} \|v - \hat{\mathcal{I}} v\|_{L_2(\hat{\kappa})} + \|\nabla (v - \hat{\mathcal{I}} v)\|_{L_2(\hat{\kappa})} \leq C \|\nabla v\|_{L_2(\hat{\kappa})},$$

where C is a positive constant, which is independent of the local mesh size $h_{\hat{\kappa}}$ and the local polynomial degree $p_{\hat{\kappa}}$.

Proof. See [17] and the references cited therein, for example. □

Given the operator $\hat{\mathcal{I}}$ defined in Lemma 5.7, we introduce the projection operator $\mathcal{I}$ on κ by the relation

$$\mathcal{I}v = \hat{\mathcal{I}}(\mathfrak{E}v)|_{\kappa}, \tag{5.6}$$

where $\mathfrak{E}$ denotes the extension operator defined in Theorem 2.1. With this notation, we state the following approximation result.

LEMMA 5.8. *Given $\kappa \in \mathcal{T}_{\mathtt{CFE}}$, let $F \subset \partial\kappa$ denote one of its faces. For a function $v \in H^1(\kappa)$, the following bound holds*

$$h_\kappa^{-1}p_\kappa\|v-\mathcal{I}v\|_{L_2(\kappa)} + \|\nabla(v-\mathcal{I}v)\|_{L_2(\kappa)} + h_F^{1/2}h_\kappa^{-1}p_\kappa^{1/2}\|v-\mathcal{I}v\|_{L_2(F)} \leq C\|\nabla\mathfrak{E}v\|_{L_2(\hat{\kappa})},$$

where $p_\kappa \geq 1$ and C is a positive constant, independent of v and the discretization parameters.

Proof. We first consider the proof of the upper bounds on the $L_2(\kappa)$ norms of $v-\mathcal{I}v$ and $\nabla(v-\mathcal{I}v)$. Exploiting Lemma 5.7, we immediately deduce that

$$\begin{aligned} &h_\kappa^{-1}p_\kappa\|v-\mathcal{I}v\|_{L_2(\kappa)} + \|\nabla(v-\mathcal{I}v)\|_{L_2(\kappa)} \\ &\quad\leq h_\kappa^{-1}p_\kappa\|\mathfrak{E}v-\hat{\mathcal{I}}(\mathfrak{E}v)\|_{L_2(\hat{\kappa})} + \|\nabla(\mathfrak{E}v-\hat{\mathcal{I}}(\mathfrak{E}v))\|_{L_2(\hat{\kappa})} \leq C\|\nabla\mathfrak{E}v\|_{L_2(\hat{\kappa})}. \end{aligned} \tag{5.7}$$

The proof of the upper bound on the approximation error measured in terms of the $L_2(F)$-norm now follows immediately from the above result, together with the multiplicative trace inequality

$$\|v\|_{L_2(F)}^2 \leq C(\|\nabla v\|_{L_2(\kappa)}\|v\|_{L_2(\kappa)} + h_F^{-1}\|v\|_{L_2(\kappa)}^2), \tag{5.8}$$

where C is a positive independent of the meshsize. We remark, cf. [7, 4], that h_F appears in (5.8) rather than h_κ due to the general shape of the element κ. □

5.1.2. Proof of Theorem 5.1. The proof of Theorem 5.1 is based on the analytical techniques developed in [17]; an alternative proof, based on employing so-called lifting operators is presented in [15].

Exploiting the decomposition (5.4), we note that

$$\begin{aligned} |||\, e_h \,|||_{\mathtt{DG}}^2 &= \sum_{\kappa\in\mathcal{T}_{\mathtt{CFE}}} \|\nabla e_h\|_{L_2(\kappa)}^2 + \sum_{F\in\mathcal{F}(\mathcal{T}_{\mathtt{CFE}})} \|\sigma^{1/2}[\![e_h]\!]\|_{L_2(F)}^2 \\ &= \sum_{\kappa\in\mathcal{T}_{\mathtt{CFE}}}\int_\kappa \nabla e_h\cdot\nabla e_h^c d\mathbf{x} - \sum_{\kappa\in\mathcal{T}_{\mathtt{CFE}}}\int_\kappa \nabla e_h\cdot\nabla u_h^\perp d\mathbf{x} + \sum_{F\in\mathcal{F}(\mathcal{T}_{\mathtt{CFE}})}\int_F \sigma|[\![e_h]\!]|^2 ds \\ &\equiv \mathrm{T}_1 + \mathrm{T}_2 + \mathrm{T}_3. \end{aligned} \tag{5.9}$$

We now proceed to bound each of the terms T_1, T_2, and T_3 individually.

Term T_1. Exploiting integration by parts gives

$$\begin{aligned} \mathrm{T}_1 &= -\sum_{\kappa\in\mathcal{T}_{\mathtt{CFE}}}\int_\kappa \Delta u\, e_h^c d\mathbf{x} - \sum_{\kappa\in\mathcal{T}_{\mathtt{CFE}}}\int_\kappa \nabla u_h\cdot\nabla e_h^c d\mathbf{x} \\ &= \sum_{\kappa\in\mathcal{T}_{\mathtt{CFE}}}\int_\kappa f\, e_h^c d\mathbf{x} - \sum_{\kappa\in\mathcal{T}_{\mathtt{CFE}}}\int_\kappa \nabla u_h\cdot\nabla e_h^c d\mathbf{x}. \end{aligned}$$

We write $\mathcal{I}e_h^c \in V(\mathcal{T}_{\mathtt{CFE}}, \boldsymbol{p})$ to be the element-wise interpolant of e_h^c defined by (5.6). Thereby, exploiting the definition of the *hp*–DGCFEM (4.2) and integrating by parts elementwise, we get

$$\begin{aligned}
\mathrm{T}_1 = &\sum_{\kappa\in\mathcal{T}_{\mathtt{CFE}}}\int_\kappa f\,(e_h^c - \mathcal{I}e_h^c)d\mathbf{x} - \sum_{\kappa\in\mathcal{T}_{\mathtt{CFE}}}\int_\kappa \nabla u_h\cdot\nabla(e_h^c - \mathcal{I}e_h^c)d\mathbf{x}\\
&- \sum_{F\in\mathcal{F}(\mathcal{T}_{\mathtt{CFE}})}\int_F \left(\{\!\{\nabla_h u_h\}\!\}\cdot[\![\mathcal{I}e_h^c]\!] + \{\!\{\nabla_h \mathcal{I}e_h^c\}\!\}\cdot[\![u_h]\!]\right) ds\\
&+ \sum_{F\in\mathcal{F}(\mathcal{T}_{\mathtt{CFE}})}\int_F \sigma\,[\![u_h]\!]\cdot[\![\mathcal{I}e_h^c]\!]\,ds\\
= &\sum_{\kappa\in\mathcal{T}_{\mathtt{CFE}}}\int_\kappa (f+\Delta u_h)\,(e_h^c - \mathcal{I}e_h^c)d\mathbf{x} - \sum_{\kappa\in\mathcal{T}_{\mathtt{CFE}}}\int_{\partial\kappa}\frac{\partial u_h}{\partial\mathbf{n}_\kappa}(e_h^c - \mathcal{I}e_h^c)ds\\
&- \sum_{F\in\mathcal{F}(\mathcal{T}_{\mathtt{CFE}})}\int_F \left(\{\!\{\nabla_h u_h\}\!\}\cdot[\![\mathcal{I}e_h^c]\!] + \{\!\{\nabla_h \mathcal{I}e_h^c\}\!\}\cdot[\![u_h]\!]\right) ds\\
&+ \sum_{F\in\mathcal{F}(\mathcal{T}_{\mathtt{CFE}})}\int_F \sigma\,[\![u_h]\!]\cdot[\![\mathcal{I}e_h^c]\!]\,ds.
\end{aligned}$$

We now recall the following result used to transfer between element-based and face-based integrations, cf. [11]:

$$\begin{aligned}
\sum_{\kappa\in\mathcal{T}_{\mathtt{CFE}}}\int_{\partial\kappa}\frac{\partial u_h}{\partial\mathbf{n}_\kappa}(e_h^c - \mathcal{I}e_h^c)ds = &\sum_{F\in\mathcal{F}(\mathcal{T}_{\mathtt{CFE}})}\int_F \{\!\{\nabla_h u_h\}\!\}\cdot[\![e_h^c - \mathcal{I}e_h^c]\!]\,ds\\
&+ \sum_{F\in\mathcal{F}^{\mathcal{I}}(\mathcal{T}_{\mathtt{CFE}})}\int_F [\![\nabla_h u_h]\!]\{\!\{e_h^c - \mathcal{I}e_h^c\}\!\}\,ds. \quad (5.10)
\end{aligned}$$

Recalling that $e_h^c \in H_0^1(\Omega)$, it follows that $[\![e_h^c]\!]_F = \mathbf{0}$ for all $F \in \mathcal{F}(\mathcal{T}_{\mathtt{CFE}})$. Thereby,

$$\begin{aligned}
\mathrm{T}_1 = &\sum_{\kappa\in\mathcal{T}_{\mathtt{CFE}}}\int_\kappa (f+\Delta u_h)\,(e_h^c - \mathcal{I}e_h^c)d\mathbf{x} - \sum_{F\in\mathcal{F}^{\mathcal{I}}(\mathcal{T}_{\mathtt{CFE}})}\int_F [\![\nabla u_h]\!]\{\!\{e_h^c - \mathcal{I}e_h^c\}\!\}\,ds\\
&- \sum_{F\in\mathcal{F}(\mathcal{T}_{\mathtt{CFE}})}\int_F \{\!\{\nabla_h \mathcal{I}e_h^c\}\!\}\cdot[\![u_h]\!]\,ds + \sum_{F\in\mathcal{F}(\mathcal{T}_{\mathtt{CFE}})}\int_F \sigma\,[\![u_h]\!]\cdot[\![\mathcal{I}e_h^c]\!]\,ds\\
\equiv\ &\mathrm{T}_{11} + \mathrm{T}_{12} + \mathrm{T}_{13} + \mathrm{T}_{14}. \quad (5.11)
\end{aligned}$$

Proceeding as in [17], employing the Cauchy–Schwarz inequality, together with the approximation result stated in Lemma 5.8 gives

$$\begin{aligned}
\mathrm{T}_{11} &\le \left(\sum_{\kappa\in\mathcal{T}_{\mathtt{CFE}}} h_\kappa^2 p_\kappa^{-2}\|f+\Delta u_h)\|_{L_2(\kappa)}^2\right)^{1/2}\left(\sum_{\kappa\in\mathcal{T}_{\mathtt{CFE}}} h_\kappa^{-2} p_\kappa^2\|e_h^c - \mathcal{I}e_h^c\|_{L_2(\kappa)}^2\right)^{1/2}\\
&\le C\left(\sum_{\kappa\in\mathcal{T}_{\mathtt{CFE}}} h_\kappa^2 p_\kappa^{-2}\|f+\Delta u_h)\|_{L_2(\kappa)}^2\right)^{1/2}\|\nabla\mathfrak{E}e_h^c\|_{L_2(\Omega_H)}. \quad (5.12)
\end{aligned}$$

Analogously, exploiting Lemma 5.8 and Assumption (A1), we deduce that

$$\begin{aligned}\mathrm{T}_{12} &\leq \left(\sum_{\kappa\in\mathcal{T}_{\mathtt{CFE}}}\sum_{F\subset\partial\kappa\setminus\partial\Omega} h_\kappa^2 h_F^{-1}p_\kappa^{-1}\|[\![\nabla u_h]\!]\|_{L_2(F)}^2\right)^{1/2}\\ &\qquad\times\left(\sum_{\kappa\in\mathcal{T}_{\mathtt{CFE}}}\sum_{F\subset\partial\kappa\setminus\partial\Omega} h_\kappa^{-2}h_F p_\kappa\|e_h^c-\mathcal{I}e_h^c\|_{L_2(F)}^2\right)^{1/2}\\ &\leq C\left(\sum_{\kappa\in\mathcal{T}_{\mathtt{CFE}}}\sum_{F\subset\partial\kappa\setminus\partial\Omega} h_\kappa^2 h_F^{-1}p_\kappa^{-1}\|[\![\nabla u_h]\!]\|_{L_2(F)}^2\right)^{1/2}\|\nabla\mathfrak{E}e_h^c\|_{L_2(\Omega_H)}. \quad (5.13)\end{aligned}$$

To deal with Term T_{13}, we employ the inverse inequality (4.1), together with (A3) and (A1):

$$\begin{aligned}\mathrm{T}_{13} &\leq \left(\sum_{F\in\mathcal{F}(\mathcal{T}_{\mathtt{CFE}})}\sigma\|[\![u_h]\!]\|_{L_2(F)}^2\right)^{1/2}\left(\sum_{F\in\mathcal{F}(\mathcal{T}_{\mathtt{CFE}})}\sigma^{-1}\|\{\!\{\nabla_h\mathcal{I}e_h^c\}\!\}\|_{L_2(F)}^2\right)^{1/2}\\ &\leq C\left(\sum_{F\in\mathcal{F}(\mathcal{T}_{\mathtt{CFE}})}\sigma\|[\![u_h]\!]\|_{L_2(F)}^2\right)^{1/2}\|\nabla_h\mathcal{I}e_h^c\|_{L_2(\Omega)}.\end{aligned}$$

Exploiting Lemma 5.8, we note that

$$\|\nabla_h\mathcal{I}e_h^c\|_{L_2(\Omega)}\leq\|\nabla_h(\mathcal{I}e_h^c-e_h^c)\|_{L_2(\Omega)}+\|\nabla e_h^c\|_{L_2(\Omega)}\leq C\|\nabla\mathfrak{E}e_h^c\|_{L_2(\Omega_H)}+\|\nabla e_h^c\|_{L_2(\Omega)}$$

Thereby,

$$\mathrm{T}_{13}\leq C\left(\sum_{F\in\mathcal{F}(\mathcal{T}_{\mathtt{CFE}})}\sigma\|[\![u_h]\!]\|_{L_2(F)}^2\right)^{1/2}(\|\nabla\mathfrak{E}e_h^c\|_{L_2(\Omega_H)}+\|\nabla e_h^c\|_{L_2(\Omega)}). \quad (5.14)$$

Again, noting that $[\![e_h^c]\!]_F=\mathbf{0}$ for all $F\in\mathcal{F}(\mathcal{T}_{\mathtt{CFE}})$, recalling Assumption (A3) and exploiting Lemma 5.8 gives

$$\begin{aligned}\mathrm{T}_{14} &= \sum_{F\in\mathcal{F}(\mathcal{T}_{\mathtt{CFE}})}\int_F\sigma\,[\![u_h]\!]\cdot[\![\mathcal{I}e_h^c-e_h^c]\!]\,ds\\ &\leq\left(\sum_{F\in\mathcal{F}(\mathcal{T}_{\mathtt{CFE}})}\sigma h_\kappa^2h_F^{-2}\mathtt{p}\|[\![u_h]\!]\|_{L_2(F)}^2\right)^{1/2}\left(\sum_{F\in\mathcal{F}(\mathcal{T}_{\mathtt{CFE}})}\sigma h_\kappa^{-2}h_F^2\mathtt{p}^{-1}\|[\![\mathcal{I}e_h^c-e_h^c]\!]\|_{L_2(F)}^2\right)^{1/2}\\ &\leq C\left(\sum_{F\in\mathcal{F}(\mathcal{T}_{\mathtt{CFE}})}\sigma h_\kappa^2h_F^{-2}\mathtt{p}\|[\![u_h]\!]\|_{L_2(F)}^2\right)^{1/2}\|\nabla\mathfrak{E}e_h^c\|_{L_2(\Omega_H)}. \quad (5.15)\end{aligned}$$

Substituting the bounds (5.12)–(5.15) into (5.11) and exploiting Theorem 2.1, we deduce that

$$\begin{aligned}\mathrm{T}_1 \leq C \Bigg[&\left(\sum_{\kappa \in \mathcal{T}_{\mathtt{CFE}}} h_\kappa^2 p_\kappa^{-2} \|f + \Delta u_h)\|_{L_2(\kappa)}^2 \right)^{1/2} \\ &+ \left(\sum_{\kappa \in \mathcal{T}_{\mathtt{CFE}}} \sum_{F \subset \partial\kappa \setminus \partial\Omega} h_\kappa^2 h_F^{-1} p_\kappa^{-1} \|[\![\nabla u_h]\!]\|_{L_2(F)}^2 \right)^{1/2} \\ &+ \left(\sum_{F \in \mathcal{F}(\mathcal{T}_{\mathtt{CFE}})} \sigma h_\kappa^2 h_F^{-2} \mathtt{p} \|[\![u_h]\!]\|_{L_2(F)}^2 \right)^{1/2} \Bigg] \|\nabla e_h^c\|_{L_2(\Omega)}.\end{aligned}$$

Thereby, employing the Cauchy–Schwarz inequality and Proposition 5.6, gives

$$\mathrm{T}_1 \leq C \left(\sum_{\kappa \in \mathcal{T}_{\mathtt{CFE}}} (\eta_\kappa^2 + \mathcal{O}_\kappa^2) \right)^{1/2} |||\, e_h \,|||_{\mathtt{DG}}. \tag{5.16}$$

Term T_2. As above, employing the Cauchy–Schwarz inequality, together with Proposition 5.6, we get

$$\mathrm{T}_2 \leq \|\nabla e_h\|_{L_2(\Omega)} \|\nabla u_h^\perp\|_{L_2(\Omega)} \leq C \left(\sum_{\kappa \in \mathcal{T}_{\mathtt{CFE}}} \eta_\kappa^2 \right)^{1/2} |||\, e_h \,|||_{\mathtt{DG}}. \tag{5.17}$$

Term T_3. Noting that $u \in H_0^1(\Omega)$ gives

$$\mathrm{T}_3 = \sum_{F \in \mathcal{F}(\mathcal{T}_{\mathtt{CFE}})} \int_F \sigma [\![e_h]\!] \cdot [\![u_h]\!] ds \leq \left(\sum_{\kappa \in \mathcal{T}_{\mathtt{CFE}}} \eta_\kappa^2 \right)^{1/2} |||\, e_h \,|||_{\mathtt{DG}}. \tag{5.18}$$

Inserting the bounds (5.16), (5.17), and (5.18) into (5.9) and dividing both sides by $|||\, e_h \,|||_{\mathtt{DG}}$ completes the proof of Theorem 5.1.

6. Numerical experiments. In this section we present a series of computational examples to highlight the practical performance of the *a posteriori* error bound derived in Theorem 5.1 for problems where the underlying computational domain contains micro-structures. Throughout this section the DGCFEM solution u_h defined by (4.2) is computed with the constant γ appearing in the discontinuity stabilization function σ equal to 10. All the numerical examples presented in this section have been computed using the AptoFEM package (`www.aptofem.com`); furthermore the resulting system of linear equations are solved based on employing the Multifrontal Massively Parallel Solver (MUMPS), see [1, 2, 3].

Algorithm 6.1 outlines the general adaptive algorithm employed within this section. In particular, we point out that the elements are marked for refinement/derefinement, according to the size of the local error indicators η_κ, based on employing the fixed fraction refinement strategy; here, we set the refinement and derefinement fractions θ_r and θ_d, respectively, equal to 25% and 5%, respectively. Once an element $\kappa \in \mathcal{T}_{\mathtt{CFE}}$ has been marked for refinement/derefinement, we employ the *hp*–adaptive strategy developed in [16] to decide whether *h*– or *p*–refinement/derefinement should

Algorithm 6.1 Adaptive Refinement Algorithm

Input parameters: refinement/derefinement fractions θ_r and θ_d, respectively; termination tolerance tol; maximum number of refinement steps $k_{\texttt{max}}$.
Initial step: Input initial composite finite element mesh $\mathcal{T}_{\texttt{CFE}}$ and reference mesh $\hat{\mathcal{T}}_{h_\ell}$, cf. Algorithm 3.1, and select initial polynomial degree distribution $\boldsymbol{p}$ in order to construct the composite and reference finite element spaces $V(\mathcal{T}_{\texttt{CFE}}, \boldsymbol{p})$ and $V(\hat{\mathcal{T}}_{h_\ell}, \hat{\boldsymbol{p}})$, respectively.
Set $V(\mathcal{T}_{\texttt{CFE}_1}, \boldsymbol{p}_1) = V(\mathcal{T}_{\texttt{CFE}}, \boldsymbol{p})$ and the mesh counter $k = 1$.
while $k < k_{\texttt{max}}$ **do**
    Compute $u_h \in V(\mathcal{T}_{\texttt{CFE}_k}, \boldsymbol{p}_k)$, cf. (4.2).
    Evaluate the error indicators η_κ, defined by (5.2), for all $\kappa \in \mathcal{T}_k$
    if $C\left(\sum_{\kappa \in \mathcal{T}_{\texttt{CFE}_k}} (\eta_\kappa^2 + \mathcal{O}_\kappa^2)\right)^{1/2} <$ tol **then**
        Exit.
    else
        Mark elements for refinement/derefinement employing the fixed fraction refinement strategy with refinement and derefinement fractions θ_r and θ_d, respectively.
        if Element κ is marked for refinement/derefinement **then**
            Perform hp–refinement/derefinement based on testing the smoothness of the computed solution u_h; see, e.g., [16, 8].
        end if
        Set $k = k + 1$ and generate the new composite finite element space $V(\mathcal{T}_{\texttt{CFE}_k}, \boldsymbol{p}_k)$.
        hp–Refine the reference finite element space $V(\hat{\mathcal{T}}_{h_\ell}, \hat{\boldsymbol{p}})$ (if necessary), to ensure that the inclusion $V(\mathcal{T}_{\texttt{CFE}_k}, \boldsymbol{p}_k) \subseteq V(\hat{\mathcal{T}}_{h_\ell}, \hat{\boldsymbol{p}})$ holds.
    end if
end while

be performed on κ; for related work, we refer to [8, 26], for example, and the review article [20]. Finally, we remark that to ensure that the inclusion $V(\mathcal{T}_{\texttt{CFE}_k}, \boldsymbol{p}_k) \subseteq V(\hat{\mathcal{T}}_{h_\ell}, \hat{\boldsymbol{p}})$ remains valid as the adaptive algorithm proceeds, subsequent refinement of the (finest) reference finite element space $V(\hat{\mathcal{T}}_{h_\ell}, \hat{\boldsymbol{p}})$ may need to be undertaken. Indeed, additional refinement is performed to ensure that the following two conditions hold:

1. Given any element $\kappa \in \mathcal{T}_{\texttt{CFE}}$, we may write $\kappa = \cup \kappa_\ell$, $\kappa_\ell \in \mathcal{S}_\kappa$, where $\mathcal{S}_\kappa$ denotes a subset of elements which belong to $\hat{\mathcal{T}}_{h_\ell}$.
2. Given $\kappa \in \mathcal{T}_{\texttt{CFE}}$ and the corresponding set $\mathcal{S}_\kappa = \{\hat{\kappa} \in \hat{\mathcal{T}}_{h_\ell} : \hat{\kappa} \subset \kappa\}$ consisting of fine level reference elements which form κ, we require that the polynomial degree $p_{\hat{\kappa}}$ defined for each $\hat{\kappa} \in \mathcal{S}_\kappa$ is set equal to the polynomial degree p_κ of the composite element κ, i.e., $p_{\hat{\kappa}} = p_\kappa$ for all $\hat{\kappa} \in \mathcal{S}_\kappa$.

6.1. Example 1: Square domain with micro-structures. In this first example, we consider the case when the computational domain Ω contains a large number of small geometric features. To this end, we set Ω to be the unit square $(0,1)^2$ in two–dimensions, which has had a series of uniformly spaced square holes removed; here, we consider the case where 256 small square holes are removed from $(0,1)^2$, cf. [5]. In this example, we select the right-hand side forcing function f and an appropriate inhomogeneous boundary condition $u = g$ on $\partial\Omega$, so that the analytical solution is

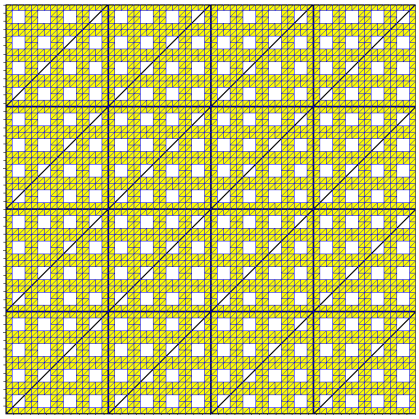

FIG. 6.1. *Example 1: Initial composite finite element mesh consisting of 32 elements, together with the initial fine level reference mesh consisting of 6144 elements.*

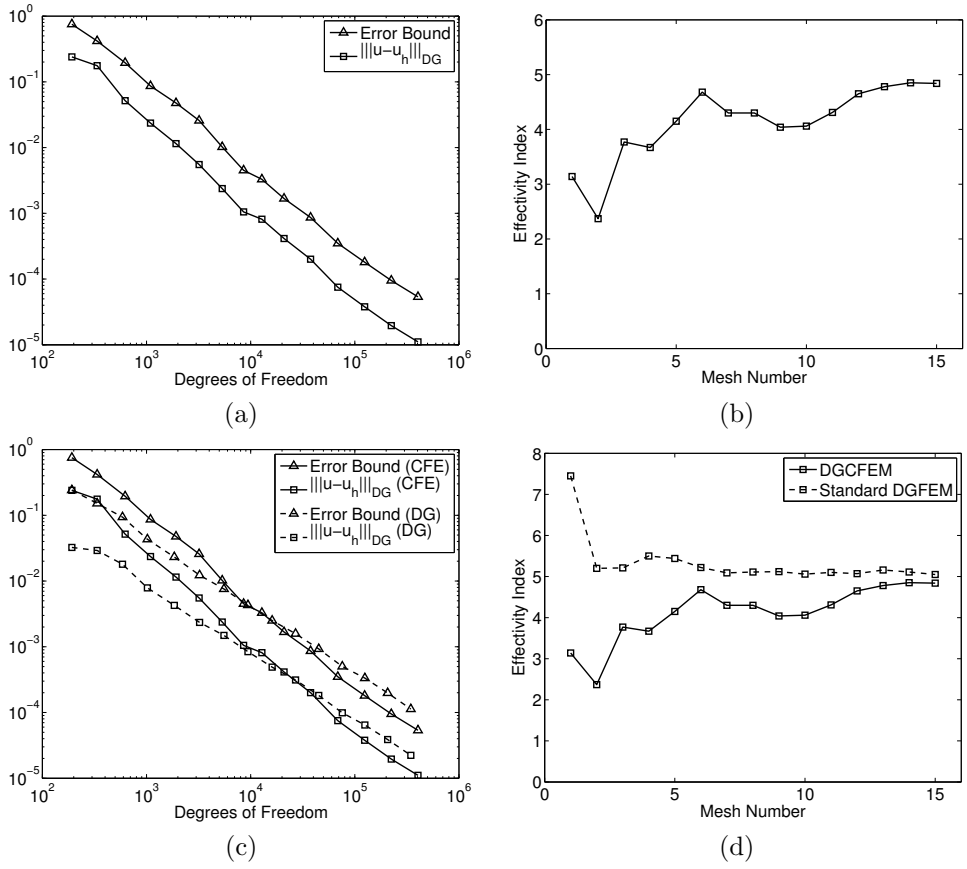

FIG. 6.2. *Example 1: Adaptive algorithm employing h–refinement with* $\boldsymbol{p} = \mathbf{2}$. *(a) Comparison of actual and estimated energy norm of the error with respect to the number of degrees of freedom; (b) Effectivity indices; (c) Comparison between DGCFEM and the standard DGFEM (computed without any holes); (d) Effectivity indices for DGCFEM and DGFEM.*

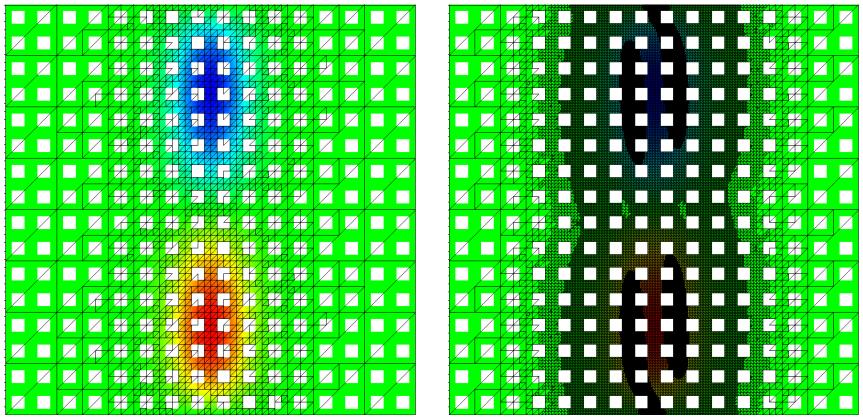

(a) (b)

FIG. 6.3. *Example 1: Adaptive algorithm employing h–refinement with* $\boldsymbol{p} = \mathbf{2}$. *h–Mesh (and solution) after: (a) 7 adaptive refinements with 1426 elements; (b) 13 adaptive refinements, with 37355 elements.*

given by

$$u(x,y) = x(1-x)y(1-y)(1-2y)\,\mathrm{e}^{-s(2x-1)^2},$$

where s is a positive constant, cf. [15, 19]; throughout this section we set $s = 25$.

In order to compute the numerical approximation to (2.1)–(2.2) (subject to inhomogeneous Dirichlet boundary conditions), using the DGCFEM defined in (4.2), we first construct a sequence of meshes based on employing Algorithm 3.1 outlined in Section 3. To this end, the coarsest reference mesh $\hat{\mathcal{T}}_H$ is selected to be a uniform triangular mesh; in particular, $\hat{\mathcal{T}}_H$ is constructed from a uniform 4×4 square mesh by connecting the north east vertex with the south west one within each mesh square. This mesh is then subsequently adaptively refined in order to generate a fine reference mesh $\hat{\mathcal{T}}_\ell$ consisting of 6144 triangular elements, which precisely describes the computational domain Ω, cf. Figure 6.1; thereby, the initial composite finite element mesh $\mathcal{T}_{\mathtt{CFE}}$ simply consists of 32 elements.

We first begin by considering the performance of the proposed *a posteriori* error estimators with h–refinement, i.e., the polynomial degrees are kept fixed; here, we set $\boldsymbol{p} = \mathbf{2}$, i.e., piecewise discontinuous quadratic polynomials are employed. To this end, in Figure 6.2(a) we present a comparison of the actual and estimated energy norm of the error versus the number of degrees of freedom in the composite finite element space $V(\mathcal{T}_{\mathtt{CFE}}, \boldsymbol{p})$ for the sequence of meshes generated by Algorithm 6.1 (with fixed polynomial degrees). Here, we observe that the error bound over-estimates the true error by a (reasonably) consistent factor; indeed, from Figure 6.2(b), we see that the computed effectivity indices tend to a value just below 5. In order to assess the quality of the computed DGCFEM solution on adaptively refined composite meshes, in Figure 6.2(c) we compare the proposed DGCFEM with the standard DGFEM; in the latter case, we simply compute the numerical solution on the unit square $(0,1)^2$ *without* any holes, cf. [4], using the error indicators derived in [15]. Here, we now observe that the accuracy and rate of convergence of the DGCFEM, which takes into account the holes present in the computational domain, is very similar to the standard DGFEM which cannot treat the micro-structures present in Ω on such coarse meshes. Indeed, this

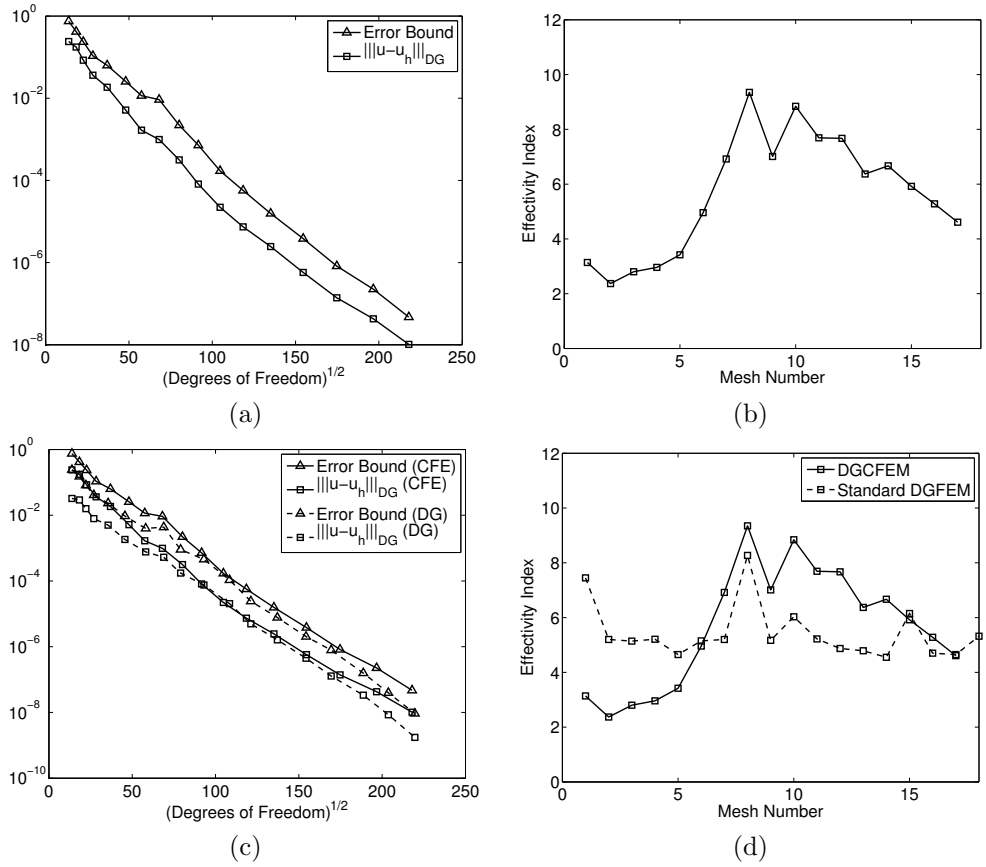

FIG. 6.4. *Example 1: Adaptive algorithm employing hp–refinement. (a) Comparison of actual and estimated energy norm of the error with respect to the square root of the number of degrees of freedom; (b) Effectivity indices; (c) Comparison between DGCFEM and the standard DGFEM (computed without any holes); (d) Effectivity indices for DGCFEM and DGFEM.*

clearly illustrates that the presence of holes/micro-structures in the computational domain does not lead to a degradation in the quality of the computed solution when the DGCFEM is exploited, cf. [4]. The effectivity indices for both methods are presented in Figure 6.2(d); here, we observe that the efficiency of both methods is very similar as the mesh is adaptively refined. In Figure 6.3, we show the composite finite element meshes generated using our *a posteriori* error indicator after 7 and 13 adaptive refinement steps. Here, we observe that h–refinement has been performed in the vicinity of the exponential 'hills' situated in the middle of the domain where the gradient/curvature of the analytical solution is relatively large.

Finally, we turn our attention to hp–adaptivity; to this end in Figure 6.4 we present analogous results to those presented in Figure 6.2 for h–refinement. In particular, in Figure 6.4(a) we present a comparison of the actual and estimated energy norm of the error versus the square root of the number of degrees of freedom in $V(\mathcal{T}_{\mathtt{CFE}}, \boldsymbol{p})$ on a linear–log scale. Here, the convergence lines using hp–refinement are roughly straight on a linear-log scale, which indicates that exponential convergence is attained for this smooth problem. The comparison with the standard DGFEM (computed on $(0,1)^2$ without any holes) again indicates that the presence of the holes

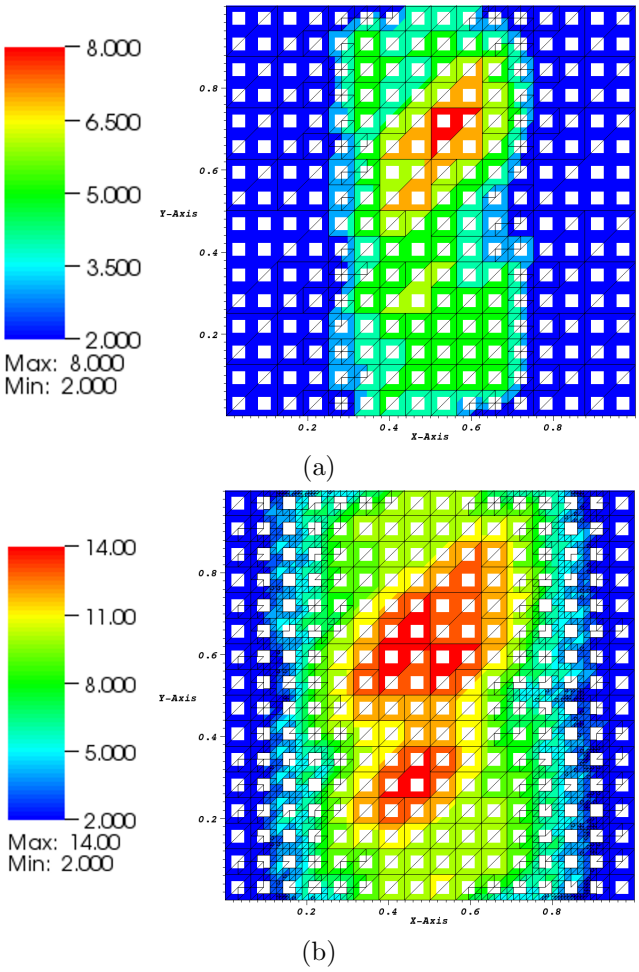

FIG. 6.5. *Example 1: Adaptive algorithm employing hp–refinement. hp–Mesh distribution after: (a) 7 adaptive refinements with 416 elements and 4639 degrees of freedom; (b) 16 adaptive refinements, with 2303 elements and 47499 degrees of freedom.*

in Ω does not lead to a degradation of the DGCFEM, cf. Figure 6.2(c). The effectivity indices shown in Figures 6.4(b) & (d) demonstrate the efficiency of the proposed error estimator. Finally, Figure 6.5 presents the *hp*–meshes after 7 and 16 adaptive refinements. As before, we observe that some *h*–refinement of the mesh has been performed in the vicinity of the base of the exponential hills situated in the left- and the right-hand sides of the domain. However, once the *h*–mesh has adequately captured the structure of the solution, the *hp*–adaptive algorithm increased the degree of the approximating polynomial within the interior part of the domain containing these hills.

6.2. Example 2: L–Shaped domain with micro-structures. In this section we let Ω be the L-shaped domain $(-1,1)^2 \setminus [0,1) \times (-1,0]$ which has had 192 square holes removed. Writing (r,φ) to denote the system of polar coordinates, we set $f = 0$

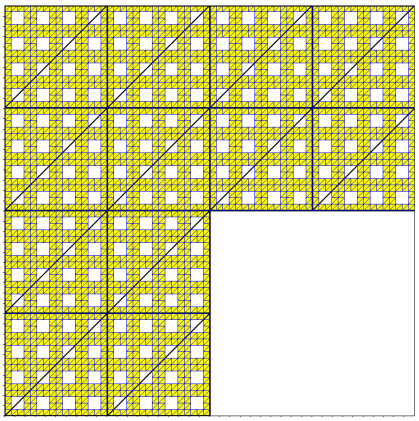

FIG. 6.6. *Example 2: Initial composite finite element mesh consisting of 24 elements, together with the initial fine level reference mesh consisting of 4608 elements.*

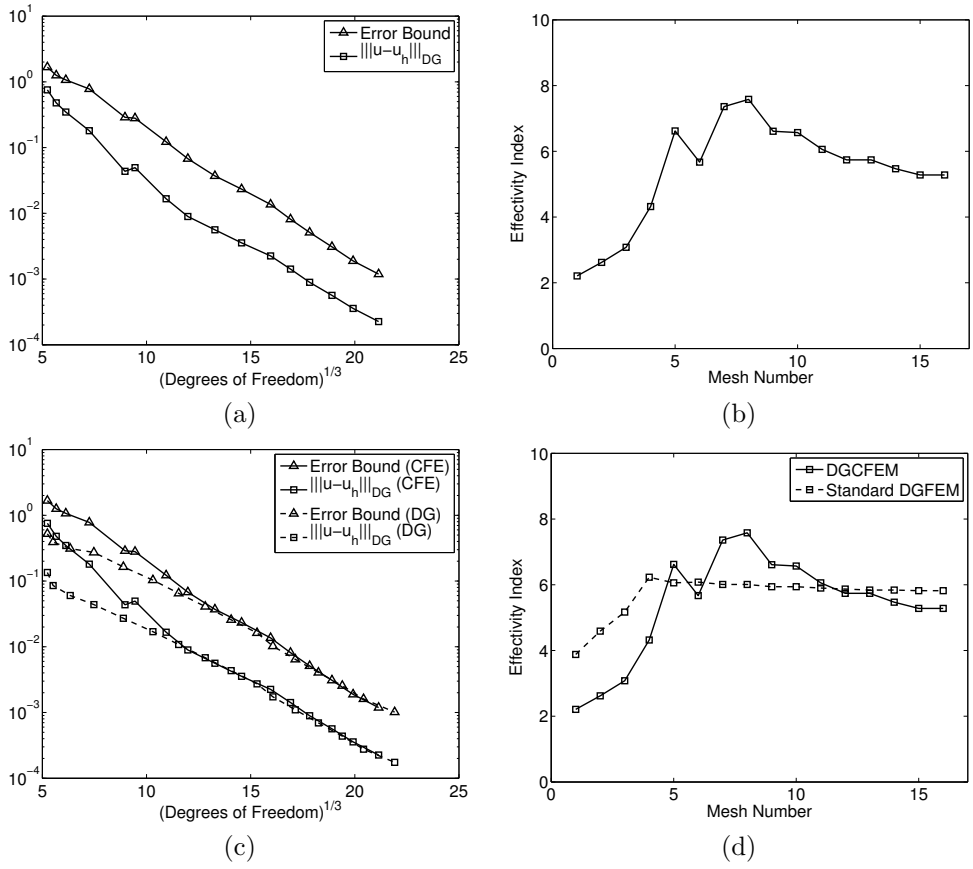

FIG. 6.7. *Example 2: Adaptive algorithm employing hp–refinement. (a) Comparison of actual and estimated energy norm of the error with respect to the (third root of the) number of degrees of freedom; (b) Effectivity indices; (c) Comparison between DGCFEM and the standard DGFEM (computed without any holes); (d) Effectivity indices for DGCFEM and DGFEM.*

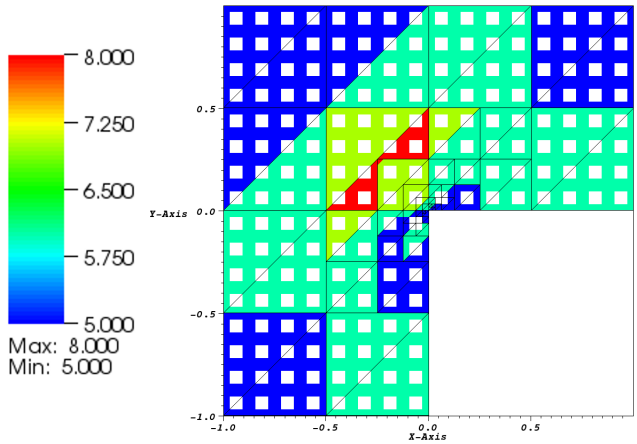

(a)

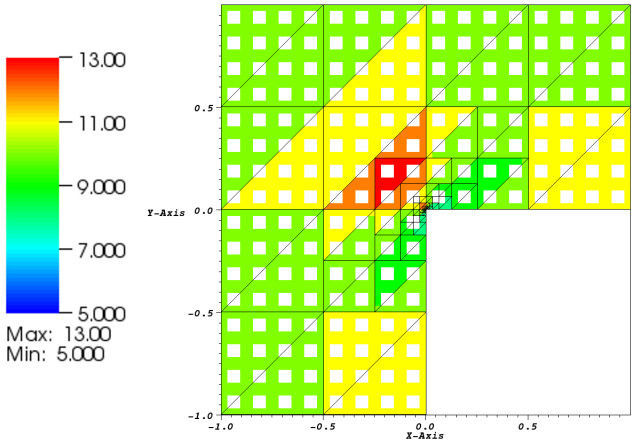

(b)

FIG. 6.8. *Example 2: Adaptive algorithm employing hp–refinement. hp–Mesh distribution after: (a) 7 adaptive refinements with 75 elements and 1722 degrees of freedom; (b) 15 adaptive refinements, with 198 elements and 9461 degrees of freedom.*

and impose an appropriate inhomogeneous boundary condition for u so that

$$u = r^{2/3} \sin(2\varphi/3);$$

cf. [27]. We note that although the boundary conditions imposed on the holes ensure that u is smooth inside $(-1,1)^2 \setminus [0,1) \times (-1,0]$, ∇u is singular at the origin; indeed, here $u \notin H^2(\Omega)$.

Here, the initial coarse reference mesh $\hat{\mathcal{T}}_H$ is selected to be a uniform triangular mesh, consisting of 24 elements, constructed as in the previous example. As before, this mesh is then adaptively refined to generate a fine reference mesh consisting of 4608 triangular elements, cf. Figure 6.6.

For brevity, in this example, we focus our attention on *hp*–mesh adaptation. Figure 6.7(a) shows the history of the actual and estimated energy norm of the error on each of the meshes generated by our *hp*–adaptive algorithm. As in the previous example, we observe that the *a posteriori* bound over-estimates the true error by a

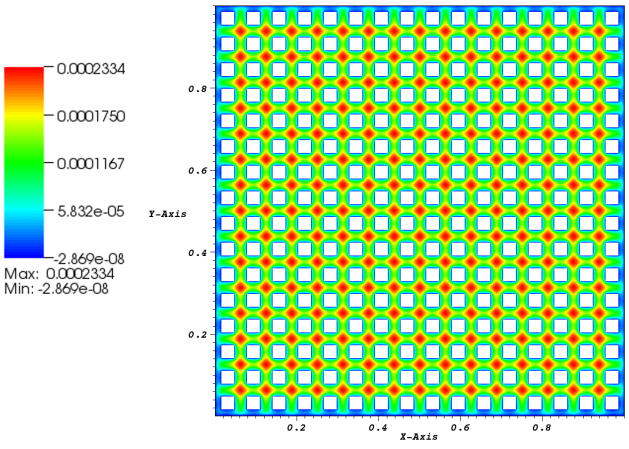

(a)

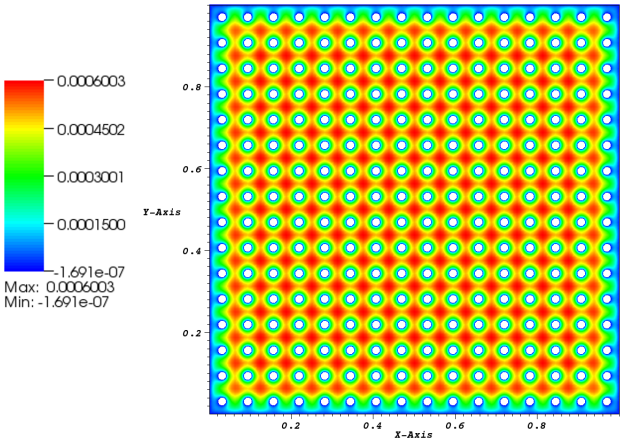

(b)

FIG. 6.9. *Example 3: Computed solution. (a) Ω contains 256 square holes; (b) Ω contains 256 circular holes.*

consistent factor; the effectivity index tends to a value of just under 6, cf. Figure 6.7(b). In addition, from Figure 6.7(a) we observe exponential convergence of the energy norm of the error using *hp*–refinement; indeed, on a linear-log scale, the convergence lines are on average straight. Figure 6.7(c) presents a comparison between the proposed DGCFEM with the standard DGFEM; as before, the latter scheme is computed on the L-shaped domain $(-1,1)^2\backslash[0,1)\times(-1,0]$ *without* any holes. As noted above, we observe that the presence of holes/micro-structures in the computational domain does not lead to a degradation in the quality of the computed solution when the DGCFEM is exploited. The effectivity indices for both methods are presented in Figure 6.7(d).

In Figure 6.8 we show the mesh generated using the local error indicators η_κ after 7 and 15 *hp*–adaptive refinement steps. Here, we see that the *h*–mesh has been largely refined in the vicinity of the re-entrant corner located at the origin; additionally, we see that the polynomial degrees have been increased away from the origin, since the underlying analytical solution is smooth in this region, cf. [15].

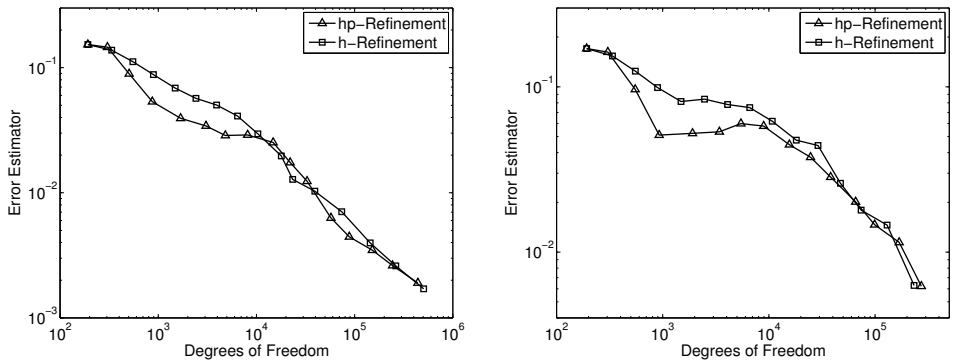

FIG. 6.10. *Example 3: Adaptive algorithm employing both h– and hp–refinement. (a) Ω contains 256 square holes; (b) Ω contains 256 circular holes.*

6.3. Example 3: Problem with representative regularity. In this final example, we again consider the case when Ω is the unit square $(0,1)^2$ in two–dimensions, which has had a series of uniformly spaced holes removed. In particular, we shall consider the two cases of when either 256 square or 256 circular holes have been removed from $(0,1)^2$. We select the right-hand side forcing function $f = 1$ and impose the homogeneous boundary condition $u = 0$ on $\partial\Omega$. Thereby, the analytical solution u contains small microstructure details, and moreover, in the case when the holes are square, reentrant corner singularities at each corner of the removed holes. The (computed) analytical solutions are depicted in Figure 6.9.

Here, the initial coarse reference mesh $\hat{\mathcal{T}}_H$ is selected to be a uniform triangular mesh, consisting of 32 elements, constructed as in Example 1. For the case of square holes, this mesh is then adaptively refined to generate a fine reference mesh consisting of 6144 triangular elements, cf. Example 1; when Ω contains circular holes, we construct a fine reference mesh consisting of 85500 elements. Given that the analytical solution is unknown in both cases, in Figure 6.10 we present a comparison between the *a posteriori* error estimator $\left(\sum_{\kappa\in\mathcal{T}_{\text{CFE}}}\eta_\kappa^2\right)^{1/2}$ computed using both *h*– and *hp*–refinement in the cases when either square or circular holes are present in Ω. Here, we observe that both mesh refinement strategies lead to very similar estimated errors for a given number of degrees of freedom; this is expected given the nature of the analytical solutions to the problems under consideration. Finally, in Figure 6.11 we show the *hp*–meshes generated using the proposed adaptive algorithm. Here we observe that while some *p*–enrichment has been undertaken, significant mesh refinement in the vicinity of the holes present in Ω has occurred.

7. Concluding remarks. In this article we have derived an energy norm *hp–a posteriori* error bound for the composite version of the discontinuous Galerkin discretization of second–order elliptic partial differential equations. This class of schemes naturally allows for the approximation of problems posed on so-called complicated domains using relatively coarse finite element spaces. Numerical examples employing both *h*– and *hp*–refinement on domains containing a large number of holes have been presented. Future work will be devoted to the consideration of more complex fluid flow problems; for related work on the application of CFEs to the Stokes equations of incompressible fluid flow, we refer to [21, 22].

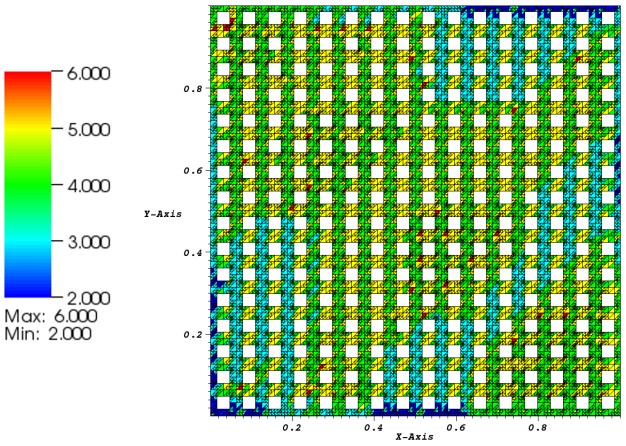

(a)

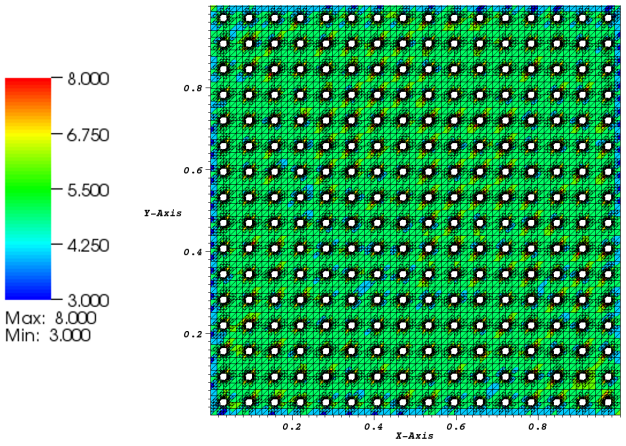

(b)

FIG. 6.11. *Example 3: Adaptive algorithm employing hp–refinement. hp–Mesh distribution for: (a) Ω contains 256 square holes, after 15 adaptive refinements with 26928 elements and 440849 degrees of freedom; (b) Ω contains 256 circular holes, after 18 adaptive refinements with 81001 elements and 1827834 degrees of freedom.*

Acknowledgements. SG and PH acknowledge the financial support of the EPSRC under the grant EP/H005498. PH also acknowledges the support of the Leverhulme Trust.

REFERENCES

[1] P. R. Amestoy, I. S. Duff, J. Koster, and J.-Y. L'Excellent. A fully asynchronous multifrontal

solver using distributed dynamic scheduling. *SIAM J. Matrix Anal. Appl.*, 23(1):15–41, 2001.

[2] P. R. Amestoy, I. S. Duff, and J.-Y. L'Excellent. Multifrontal parallel distributed symmetricand unsymmetric solvers. *Comput. Methods Appl. Mech. Eng.*, 184:501–520, 2000.

[3] P. R. Amestoy, A. Guermouche, J.-Y. L'Excellent, and S. Pralet. Hybrid scheduling for the parallel solution of linear systems. *Parallel Computing*, 32(2):136–156, 2006.

[4] P.F. Antonietti, S. Giani, and P. Houston. *hp*–Version composite discontinuous Galerkin methods for elliptic problems on complicated domains. *SIAM J. Sci. Comput.*, 35(3):A1417–A1439, 2013.

[5] P.F. Antonietti, S. Giani, and P. Houston. Domain decomposition preconditioners for discontinuous Galerkin methods for elliptic problems on complicated domains. *J. Sci. Comput.*, In press.

[6] A. Cangiani, E.H. Georgoulis, and P. Houston. *hp*-Version discontinuous Galerkin methods on polygonal and polyhedral m eshes. *Submitted for publication*, 2013.

[7] V. Dolejší, M. Feistauer, and C. Schwab. A finite volume discontinuous Galerkin scheme for nonlinear convection diffusion problems. *Calcolo*, 39:140, 2002.

[8] T. Eibner and J.M. Melenk. An adaptive strategy for hp-FEM based on testing for analyticity. *Comp. Mech.*, 39:575–595, 2007.

[9] W. Hackbusch and S.A. Sauter. Composite finite elements for problems containing small geometric details. Part II: Implementation and numerical results. *Comput. Visual Sci.*, 1:15–25, 1997.

[10] W. Hackbusch and S.A. Sauter. Composite finite elements for the approximation of PDEs on domains with complicated micro-structures. *Numer. Math.*, 75:447–472, 1997.

[11] R. Hartmann. Numerical analysis of higher order discontinuous Galerkin finite element methods. In H. Deconinck, editor, *VKI LS 2008-08: CFD - ADIGMA course on very high order discretization methods, Oct. 13-17, 2008*. Von Karman Institute for Fluid Dynamics, Rhode Saint Genèse, Belgium, 2008.

[12] P. Houston, I. Perugia, and D. Schötzau. Mixed discontinuous Galerkin approximation of the Maxwell operator. *SIAM J. Numer. Anal.*, 42:434–459, 2004.

[13] P. Houston, D. Schötzau, and T. Wihler. Energy norm a posteriori error estimation for mixed discontinuous Galerkin approximations of the Stokes problem. *J. Sci. Comput.*, 22(1):357–380, 2005.

[14] P. Houston, D. Schötzau, and T. P. Wihler. An *hp*-adaptive mixed discontinuous Galerkin FEM for nearly incompressible linear elasticity. *Comput. Methods Appl. Mech. Engrg.*, 195(25-28):3224–3246, 2006.

[15] P. Houston, D. Schötzau, and T. P. Wihler. Energy norm a posteriori error estimation of *hp*-adaptive discontinuous Galerkin methods for elliptic problems. *Math. Models Methods Appl. Sci.*, 17(1):33–62, 2007.

[16] P. Houston and E. Süli. A note on the design of *hp*-adaptive finite element methods for elliptic partial differential equations. *Comput. Methods Appl. Mech. Engrg.*, 194(2–5):229–243, 2005.

[17] P. Houston, E. Süli, and T.P. Wihler. A posteriori error analysis of *hp*-version discontinuous Galerkin finite-element methods for second-order quasi-linear PDEs. *IMA J. Numer. Anal.*, 28(2):245–273, 2007.

[18] O.A. Karakashian and F. Pascal. A posteriori error estimation for a discontinuous Galerkin approximation of second order elliptic problems. *SIAM J. Numer. Anal.*, 41:2374–2399, 2003.

[19] J.M. Melenk and B.I. Wohlmuth. On residual-based a posteriori error estimation in *hp*-FEM. *Adv. Comp. Math.*, 15:311–331, 2001.

[20] W.F. Mitchell and M.A. McClain. A comparison of *hp*–adaptive strategies for elliptic partial differential equations. *Submitted for publication*, 2012.

[21] D. Peterseim and S. Sauter. The composite mini element - coarse mesh computation of Stokes flows on complicated domains. *SIAM J. Numer. Anal.*, 46(6):3181–3206, 2008.

[22] D. Peterseim and S. Sauter. Finite element methods for the Stokes problem on complicated domains. *Comput. Methods Appl. Mech. Engrg.*, 200(33-36):2611–2623, 2011.

[23] M. Rech, S. Sauter, and A. Smolianski. Two-scale composite finite element method for the Dirichlet problem on complicated domains. *Numer. Math.*, 102(4):681–708, 2006.

[24] S. A. Sauter and R. Warnke. Extension operators and approximation on domains containing small geometric details. *East-West J. Numer. Math.*, 7(1):61–77, 1999.

[25] E. M. Stein. *Singular Integrals and Differentiability Properties of Functions*. Princeton, University Press, Princeton, N.J., 1970.

[26] T.P. Wihler. An *hp*-adaptive strategy based on continuous Sobolev embedding. *J. Com-*

put. Appl. Math., 235:2731–2739, 2011.

[27] T.P. Wihler, P. Frauenfelder, and C. Schwab. Exponential convergence of the *hp*-DGFEM for diffusion problems. *Comput. Math. Appl.*, 46:183–205, 2003.

[28] L. Zhu, S. Giani, P. Houston, and D. Schötzau. Energy norm a posteriori error estimation for *hp*-adaptive discontinuous Galerkin methods for elliptic problems in three dimensions. *Math. Model. Methods Appl. Sci.*, 21(2):267–306, 2011.

[29] L. Zhu and D. Schötzau. A robust a posteriori error estimate for *hp*–adaptive DG methods for convection-diffusion equations. *IMA J. Numer. Anal.*, 31(3):971–1005, 2010.